AGU100 ADVANCING EARTH AND SPACE SCIENCE

JGR Oceans

RESEARCH ARTICLE
10.1029/2019JC015032

Key Points:
- Robust mean and seasonal cycles of velocity and isotherm displacement data allow study of deep equatorial Pacific interannual variability
- A deep Rossby wave-like interannual signal in isotherm depths with vertical mode 3–4 is highly correlated with Niño3.4
- At 1,000 dbar residual Rossby wave-like zonal velocity signatures are less robust and not clearly related to Niño3.4

Supporting Information:
- Supporting Information S1

Correspondence to:
Hannah. Zanowski,
Hannah.Zanowski@colorado.edu

Citation:
Zanowski, H., Johnson, G. C., & Lyman, J. M. (2019). Equatorial pacific 1,000-dbar velocity and isotherm displacements from argo data: beyond the mean and seasonal cycle. *Journal of Geophysical Research: Oceans*, *124*, 7873–7882. https://doi.org/10.1029/2019JC015032

Received 5 FEB 2019
Accepted 13 OCT 2019
Accepted article online 23 OCT 2019
Published online 17 NOV 2019

Equatorial Pacific 1,000-dbar Velocity and Isotherm Displacements From Argo Data: Beyond the Mean and Seasonal Cycle

Hannah Zanowski[1], Gregory C. Johnson[2], and John M. Lyman[3,2]

[1]Joint Institute for the Study of the Atmosphere and Ocean, University of Washington, Seattle, WA, USA, [2]NOAA/Pacific Marine Environmental Lab, Seattle, WA, USA, [3]Joint Institute for Marine and Atmospheric Research, University of Hawai'i at Manoa, Honolulu, HI, USA

Abstract Equatorial Pacific zonal velocity at 1,000 dbar and vertical isotherm displacements from 0–2,000 dbar are analyzed using Argo data through February 2018. In agreement with previous studies, the mean 1,000-dbar zonal velocity is characterized by alternating eastward and westward jets of amplitude 5–10 cm/s. Similarly, the seasonal cycle is dominated by an annual Rossby wave that is apparent in annual harmonic fits to both the isotherm displacement and velocity fields. Residual (mean, annual, and semiannual harmonics removed) zonal velocity and isotherm displacements are analyzed using Complex Empirical Orthogonal Functions (CEOFs) and their Principal Components. For the analysis at 1,000 dbar, the first velocity CEOF accounts for 28% of the variance and the first isotherm displacement CEOF 24%. Spatial patterns of the lead CEOFs are broadly consistent with Rossby waves, but only isotherm displacement CEOF1 can be clearly linked to known physical processes in the equatorial Pacific. This is true of the isotherm displacement CEOF1s across pressure surfaces, despite being estimated independently on each one. The Principal Component of isotherm displacement CEOF1 at 1,000 dbar is well correlated ($r = -0.65$) with the Niño3.4 index at a 12-month lag, suggesting that El Niño signals propagate deep into the equatorial Pacific Ocean. The 3-D structure of the isotherm displacement CEOF1s suggests that the deep isotherm displacement signals are consistent with a vertically propagating Rossby wave of vertical mode 3–4.

Plain Language Summary The tropical Pacific Ocean is an important region for Earth's climate. It features a complex set of currents that exist at different depths and vary on a range of timescales from months to decades. The variations of these currents are influenced by planetary (Rossby) wave signals that travel both zonally and vertically along the equator. While it is well known that Rossby waves modulate these currents on yearly timescales, the data to observe deep current variability at longer timescales have only recently become available from the global array of Argo floats. Here we analyze velocities and isotherm displacements (vertical movements of constant temperature surfaces) from Argo float data to investigate their variations over timescales longer than a year. Using a statistical technique to find the most energetic large spatial scale and long-timescale propagating signals in these data, we demonstrate that deep isotherm displacements are highly correlated with the El Niño-Southern Oscillation (ENSO) across a large range of pressures but find that the velocities at 1,000 dbar are not. This mismatch is puzzling, but it may be due to the short record length and relatively small data set for velocity compared to the timescales of the examined velocity variations.

1. Introduction

The tropical Pacific Ocean is critically important to Earth's climate (e.g., Ropelewski and Halpert, 1987) and hosts a rich, complex set of currents with various vertical, meridional, and temporal scales. The surface-intensified westward flowing South Equatorial Current is split into a northern and southern branch near the equator, where the eastward flowing equatorial undercurrent is found, with its maximum velocity within the pycnocline (Johnson et al., 2002). The surface-intensified and eastward flowing North Equatorial Countercurrent is centered near 4°N in the west, gradually shifting northward to 6°N in the east. All of these near-surface currents exhibit substantial seasonal cycles and are modulated by the El Niño-Southern Oscillation (ENSO) as well.

Below the pycnocline, at a few hundred meters depth, are the subsurface countercurrents, or Tsuchiya Jets, that flow eastward on either side of a subsurface equatorial thermostad that contains the westward flowing

Equatorial Intermediate Current (Rowe et al., 2000). These jets shoal and shift poleward from west to east. Even below that (centered near 700 m, but with vertical extents of several hundred meters) are the eastward flowing South and North Intermediate Countercurrents and the westward flowing Lower Equatorial Intermediate Current and Southern Equatorial Intermediate Current (Firing et al., 1998).

The Equatorial Deep Jets (EDJs) are a stacked set of equatorial currents with vertical scales of a few hundred meters that are evident below the thermocline. Some of the earliest measurements of the equatorial Pacific EDJs were made in the 1970s and the early 1980s (Eriksen, 1981; Hayes & Milburn, 1980; Leetmaa & Spain, 1981; Taft et al., 1974). These new observations raised as many questions as they answered, and shortly after the Pacific Equatorial Ocean Dynamics experiment was developed in order to shed light on the zonal structure and temporal variability of the jets (Eriksen, 1985; Firing, 1987; Voorhis et al., 1984). While the data collected and other observations (e.g., Lukas & Firing, 1985; Wyrtki & Kilonsky, 1984) proved immensely useful for understanding the spatiotemporal structure of the EDJs, they were ultimately limited by their short temporal length (16 months or less). It wasn't until the late 1990s and early 2000s that there began to be enough data available to diagnose the vertical migration of the jets and their variability on longer timescales (Firing et al., 1998; Johnson et al., 2002; Youngs & Johnson, 2015). Both the EDJs and the Equatorial Intermediate Current System (EICS; Ascani et al., 2010) are important for setting the timescales of variability in the equatorial Pacific (Firing, 1987; Firing et al., 1998; Gouriou et al., 2006; Rowe et al., 2000) and for transporting a significant amount of mass, nutrients, and other biological tracers such as oxygen (Stramma et al., 2010) in the region.

A basin-scale vertically propagating annual Rossby wave (Johnson, Kunze, et al., 2002; Kessler & McCreary, 1993; Lukas & Firing, 1985; Yu & McPhaden, 1999; Yuan, 2005) with vertical and meridional mode number 1 modulates all of these currents. This wave is of sufficiently large amplitude that intermediate currents can apparently reverse sign as a result of its propagation (Gouriou et al., 2006). Modeling studies (e.g., Marin et al., 2010) show that it is also interannually modulated.

The Argo program, with its thousands of autonomous profiling floats worldwide, has vastly improved spatiotemporal data coverage in the oceans. Due to the floats' Lagrangian nature, mapping algorithms are typically employed to grid the data prior to analysis. Davis (1998, 2005) objectively mapped earlier World Ocean Circulation Experiment float drift velocities to examine the mean structure of mid-depth currents in the Pacific and Indian oceans. Cravatte et al. (2012, 2017) employed a similar method to explore the mean, seasonal cycle, and vertical structure of equatorial Pacific currents down to 2,000 m using Argo data.

While it is clear from such studies that the seasonal cycle controls much of the equatorial Pacific velocity variance, less is known from observations alone about deep velocity variability on longer timescales. Here we examine 1,000-dbar velocity and 3-D isotherm displacement data to understand the processes, such as ENSO, that impact the equatorial Pacific physical state variables at interannual and longer timescales. Despite the wealth of Argo velocity data presently available, we find that alone they are still insufficient to robustly determine the mechanisms that drive deep equatorial Pacific interannual velocity variability. Instead we focus mostly on the isotherm displacement interannual signals, as these are better sampled, more obviously connected to physical processes in the equatorial Pacific, and yield a robust signal that is coherent across a large pressure range even though the analysis is done separately on each pressure level.

2. Data and Mapping

We use Argo data for our analyses: 1,000-dbar drift velocities from YoMaHa'07 (Lebedev et al., 2007) and vertical isotherm displacements computed from Roemmich and Gilson (2009) monthly climatological fields at a set of standard pressures from 0 to 2,000 dbar, both updated through February 2018. About 52% of the 148,137 Argo float profiles available within $\pm 10°$ latitude of the equator in the Pacific from Jan. 2004 through Feb. 2018 sample to 1,950 dbar, 66% extend to 1,450 dbar, and 94% of them reach at least 950 dbar. About 75% of the 131,586 float drift trajectories available in the region from Jan. 2007 through Feb. 2018 are nominally located at 1,000 dbar. We map zonal velocities from YoMaHa'07 on a regular 0.25° lat. × 1° long. grid using a Loess filter with 1° lat. × 8° long. scales. We include annual and semiannual harmonics in the fit. We discard all drift data that fall outside 3 times the interquartile range at each point prior to mapping. We then map residual velocities (mean and harmonics removed) on a 0.25° lat. × 2° long. × 1-month grid using a Loess filter with 1.5° lat. × 12° long. × 3-month scales. Vertical isotherm displacements, denoted p', are calculated from the Roemmich and Gilson (2009) 1° lat. × 1° long. × 1-month gridded temperature fields. We convert in situ temperatures to potential temperature and scale by the local vertical temperature gradient to estimate isotherm displacement fields in pressure units (dbar). We then fit the isotherm displacement fields to mean, annual, and semiannual harmonics that we subsequently remove to create residual fields.

To assess the leading modes of variability in the residual fields, we compute Complex Empirical Orthogonal Functions (CEOFs). The fields are made complex by taking their Hilbert transform (e.g., Bouzinac et al., 1998). The velocity CEOFs are computed at 1,000 dbar using mapped data from 2007 onward. Prior to this time, the data coverage is insufficient to yield meaningful CEOF results. The residual isotherm displacements are smoothed with a 5-month Hanning filter, and then CEOFs are calculated separately at each pressure level available in the Roemmich and Gilson (2009) climatology from 2004 onward. Because we perform separate CEOF calculations for isotherm displacements at each individual pressure level, there is no mathematical reason to expect a vertically coherent signal in their first CEOFs. However, as shown below, latitude-depth and longitude-depth sections constructed from these CEOF1s for the most part exhibit remarkable coherence across a wide range of pressures. For the isotherm displacement CEOF1s and PC1s, we also present reconstructed fields on each pressure level that represent the portion of the original isotherm displacement field associated with these CEOF1s/PC1s only. This reconstruction is accomplished by multiplying isotherm displacement PC1 and CEOF1 at each pressure (and then taking the real part), resulting in a 3-D field (in lat., long., and time) in dbar, the units of the original data. (The sum of the real parts of all the reconstructed CEOF/PC fields recovers the original data.) We also compute lagged correlations between the first isotherm displacement Principal Component 1 at each pressure level and the Niño3.4 index. Prior to these calculations, we taper each time series by multiplying it with a Hanning window of length equal to that of the time series. Reported correlation values are statistically significant at the 95% confidence level.

We also estimate a vertical mode from the isotherm displacement CEOF1s. Vertical modes are inferred in part from timescales estimated using the Principal Component time series associated with the CEOFs. Assuming the WKB approximation has been made for the vertical structure, and noting that a local vertical mode (j) can be estimated from the local vertical wavenumber (m) via the equation $m = j\pi/D$, where D is the mean depth of the Pacific; the equation for the local vertical mode is

$$j = -\frac{kND}{(2n+1)\pi\omega}$$

where k is the zonal wavenumber, N is the buoyancy frequency, ω is the frequency (computed from the period, or in this case the decorrelation time, as described below), and n is the meridional mode number. For a more complete derivation, refer to the appendix of Kessler and McCreary (1993). For all calculations, we assume a first meridional mode Rossby wave ($n = 1$), a mean depth of 4,000 m, and $N = 0.0022\ s^{-1}$ for the mean buoyancy frequency (Johnson, Sloyan, et al., 2002; Youngs & Johnson, 2015) in the equatorial Pacific. Because the isotherm displacement PCs are not narrow band, in lieu of using periods to estimate their frequencies, we use estimates based on their decorrelation timescales, defined here as 2π times the maximum of the integral of the autocorrelation of the real part of each PC. These estimates would recover periods for a sinusoidal signal although the PCs are not always clearly periodic in character. Furthermore, the PC1s for the isotherm displacements do vary somewhat with pressure, further complicating the vertical mode interpretation. Because of these variations, we use a mean decorrelation timescale for the isotherm displacements, computed as the average of the PC1 decorrelation timescale at each pressure level from 200–2,000 dbar. With all these assumptions, these estimates are approximate, for rough characterizations of the temporal and spatial scales involved assuming Rossby wave-like dynamics.

3. Results

3.1. The Mean

The 1,000-dbar mean zonal velocity field is characterized by alternating eastward

and westward jets within ±20° of the equator (Figure 1). The strongest jets are nearly basin-scale in zonal extent and occur within 5–10° of the equator. In contrast, their meridional scales are quite short, about 170 km from peak eastward to peak westward velocity. These jets have amplitudes of 5–10 cm/s and, excepting the far western Pacific, are stronger and more pronounced in the Southern Hemisphere. These results are

10.1029/2019JC015032

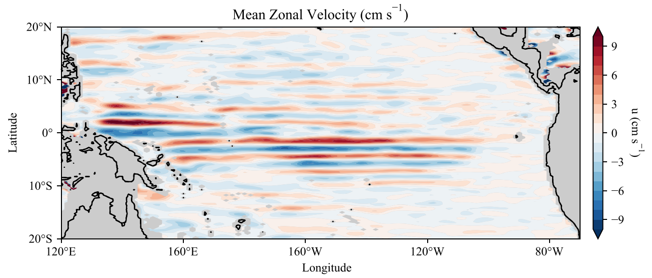

Figure 1. Equatorial Pacific mean zonal velocity (colors; cm/s) at 1,000 dbar from Loess mapping with 1° latitude × 8° longitude scales and annual and semiannual harmonics included in the fit, following Ridgway et al. (2002). Bathymetry shallower than 1,000 m is shaded gray.

consistent with the findings of Cravatte et al. (2012), who made their own calculation of the Argo drift velocities. Here we use the more extensive, although arguably less curated, YoMaHa'07 data set through February 2018. Our findings are also consistent with descriptions of Equatorial Intermediate Currents (e.g., Firing et al., 1998), with their short meridional scales, although Argo allows mapping of the weaker, higher latitude currents that were not sampled as extensively previously, as well as verifying the basin-wide zonal scales of these features at 1,000 dbar. Between 125 and 145°W and North of ~7°N, three eastward jets exist in roughly the same locations (9, 13, and 17°N) as the North Equatorial Undercurrent jets described by Qiu et al. (2013), but the magnitudes we find are somewhat weaker.

3.2. The Seasonal Cycle

The 1,000-dbar zonal velocity seasonal cycle (Figure 2) is dominated by the annual Rossby wave (e.g., Kessler & McCreary, 1993; Lukas & Firing, 1985) as expected. The annual harmonic phase (Figure 2a) is consistent with Rossby wave physics, exhibiting a basin-scale zonal structure with maximum amplitude in the western equatorial region, minimum amplitude ±2° from the equator, and a secondary off-equatorial maximum around 2.5°N. As in previous studies, the amplitudes are larger in the Northern Hemisphere than the Southern, consistent with modification by the mean upper ocean current structure (Chelton et al., 2003). Phase increases westward on the Equator, spanning the basin in about 12 months. There is also a nearly 6-month phase shift between the equatorial and off-equatorial Northern Hemisphere amplitude maximum, as expected for an annual Rossby wave, at least at longitudes where the amplitudes are large. In the Northern Hemisphere in the west, there is also some evidence for yet another phase reversal further off the equator. This feature perhaps suggests the presence of some energy at a higher meridional mode at annual timescales and has also been observed previously (Cravatte et al., 2012). The semiannual harmonic amplitude is small (Figure 2b), with velocities rarely exceeding 4 cm/s but with an orderly phase progression around the equator, suggesting a coherent signal there.

To better understand the 3-D structure of the phenomena under study here, we also examine vertical isotherm displacements calculated from the Roemmich and Gilson (2009) Argo climatology. At 1,000 dbar,

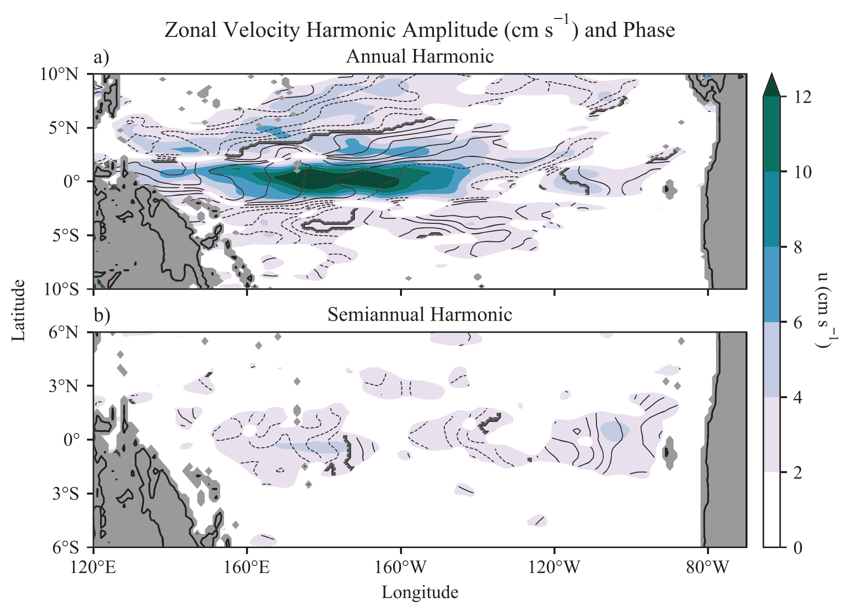

Figure 2. Zonal velocity (a) annual and (b) semiannual harmonic amplitude (colors; cm/s) and phase (contours at 30° intervals) at 1,000 dbar, mapped as in Figure 1. Phase is not shown for amplitudes less than 2 cm/s. Bathymetry shallower than 1,000 m is shaded gray.

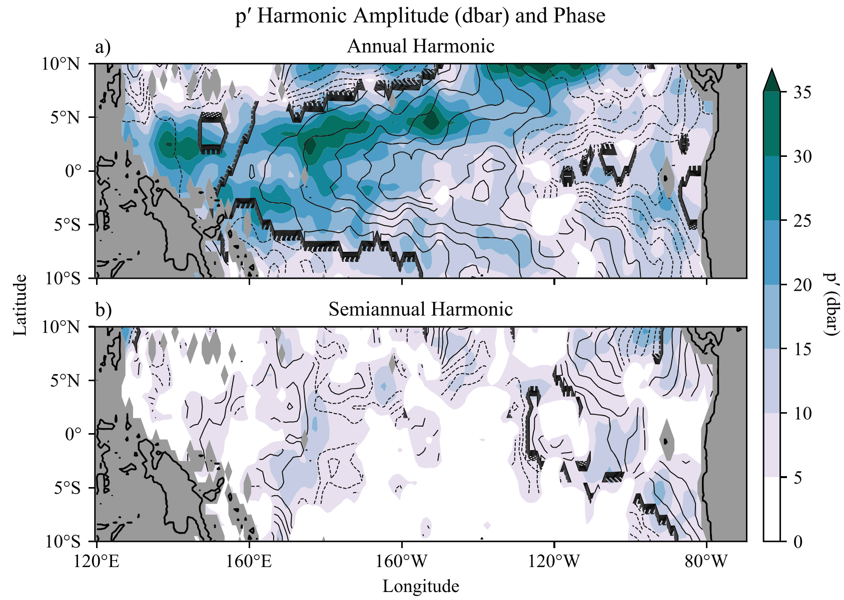

Figure 3. Isotherm displacement (a) annual and (b) semiannual harmonic amplitude (colors; dbar) and phase (contours at 30° intervals) at 1,000 dbar. Phase is not shown for amplitudes less than 5 dbar. Bathymetry shallower than 1,000 m is shaded gray.

isotherm displacement annual and semiannual harmonics (Figure 3) correspond well with the velocity annual and semiannual harmonics. The isotherm displacement annual harmonic also indicates the presence of an annual Rossby wave. It is basin-scale zonally, with a westward phase propagation spanning a year. It exhibits off-equator amplitude maxima of ~25–35 dbar centered at ±2.5° in the western and central Pacific, and phase increases poleward. It also exhibits a secondary off-equatorial poleward maximum in the Northern Hemisphere, again possibly suggesting the presence of annual Rossby wave energy at a higher meridional mode than the first. Similar to the velocity annual harmonic, the annual harmonic isotherm displacements are stronger north of the equator. The semiannual harmonic isotherm displacements are weaker overall, with amplitudes of 5–15 dbar.

Isotherm displacement pressure-longitude sections at 2.5°N highlight each harmonic's vertical structure (Figure 4). As observed in Kessler and McCreary (1993), the slope of the annual harmonic phase lines indicates upward and westward phase propagation across the basin, suggesting downward and westward energy propagation. However, with significantly more data available in our study, the upward phase propagation expected from a simple model (Kessler & McCreary, 1993) in the eastern Pacific is now much clearer, despite

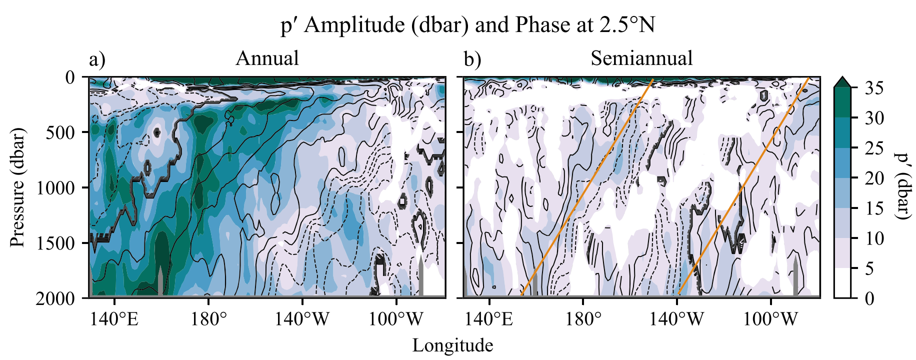

Figure 4. Isotherm displacement (a) annual and (b) semiannual harmonic amplitude (colors; dbar) and phase (contours at 30° intervals) vertical sections along 2.5°N. Phase is not shown for amplitudes less than 5 dbar. Orange lines in (b) indicate the amplitude beams described in section 3.2. Bathymetry is shaded gray.

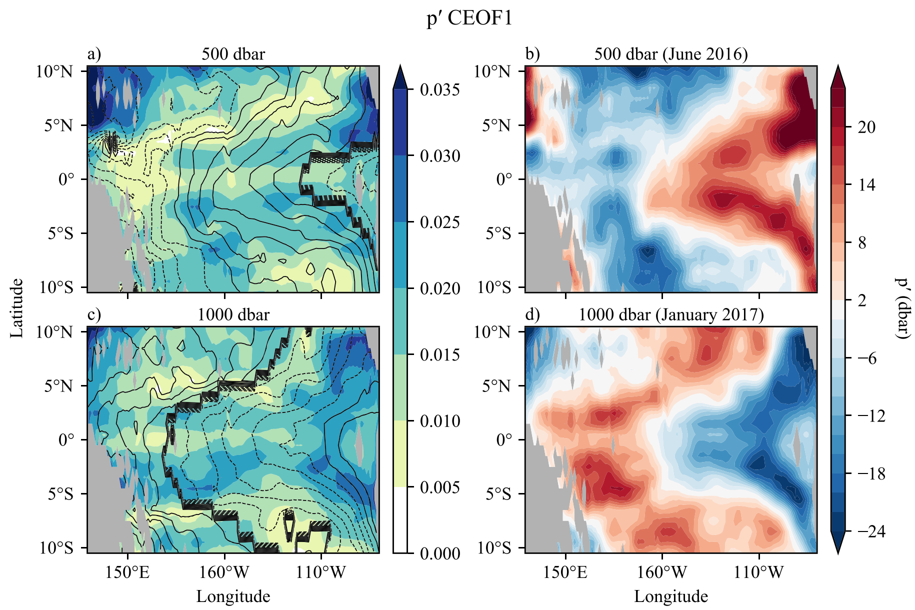

Figure 5. Isotherm displacement CEOF1 (a,c) amplitude (colors) and spatial phase (contours; 30° intervals) and (b,d) the real part of the CEOF1/PC1 reconstructions (dbar; colors) at the lags of maximum Niño3.4 correlation relative to January 2016 at (a,b) 500 dbar and (c,d) 1,000 dbar. The 500-dbar CEOF1 accounts for 27% of the residual variance and the 1,000-dbar CEOF1 24% of the residual variance. Bathymetry is shaded gray. CEOF = Complex Empirical Orthogonal Function; PC = Principal Component.

the smaller amplitude of the signal there. The semiannual harmonic analysis reveals two beams of amplitude maxima, one starting near the surface in the eastern Pacific and another in the central Pacific (Figure 4b; orange lines). While weaker and patchier than the annual harmonic results, both beams exhibit upward and westward phase propagation and descend more steeply into the deep ocean than their annual harmonic analog, as expected for their shorter period.

3.3. Interannual Variability

We employ CEOFs to analyze the residual isotherm displacement and zonal velocity variances, exploring interannual variability. At 1,000 dbar, isotherm displacement CEOF1 (Figure 5c) accounts for just under one quarter (24%) of the residual variance, and its PC is highly correlated with the Niño3.4 index with $r = -0.65$ at a 12-month lag (Figure 6). CEOF1 has features characteristic of a Rossby wave, with equatorially symmetric off-equator amplitude maxima around ±2.5° latitude that are also clear in a snapshot of the reconstructed field (Figure 5d) in January 2017 (12 months after the Niño3.4 index peaks in January 2016). The sign of the reconstructed anomalies is latitudinally dependent, with symmetric off-equator reversals at ±5° in the central Pacific (Figure 5d). Similar patterns occur at 500 dbar (Figures 5a and 5b) where isotherm displacement CEOF1 accounts for 27% of the residual variance. PC1 at 500 dbar is also correlated with the Niño3.4 index with $r = -0.82$ at a 5-month lag. Equatorially symmetric off-equator amplitude maxima are present at 2.5°N and 2.5°S (Figures 5a and 5b), and the reconstructed anomalies (Figure 5b) in June 2016 (5 months after the Niño3.4 index peaks in January 2016) exhibit symmetric off-equator sign reversals at ±5° in the central Pacific. Consistent with a downward and westward propagating Rossby wave, the 5-month lag of the 500-dbar PC1 is less than the 12-month lag of the 1,000-dbar PC1, and the location of positive anomalies occurs further west with increasing depth and time, reaching its maximum westward extent along the equator at ~140°E at 1,000 dbar versus ~170°W at 500 dbar.

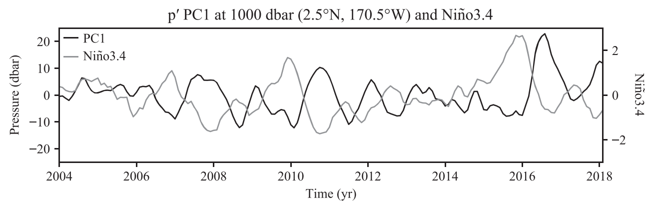

Figure 6. Time series of the real part of the reconstructed isotherm displacement CEOF1/PC1 field (black) at 1,000 dbar, 2.5°N, and 170.5°W, with the Niño 3.4 index (gray). The PC1 time series has been multiplied by its corresponding CEOF so that it has units of the original data (dbar). CEOF = Complex Empirical Orthogonal Function; PC = Principal Component.

The presence of a vertically propagating Rossby wave is further supported by isotherm displacement CEOF1 vertical sections (Figure 7)

10.1029/2019JC015032

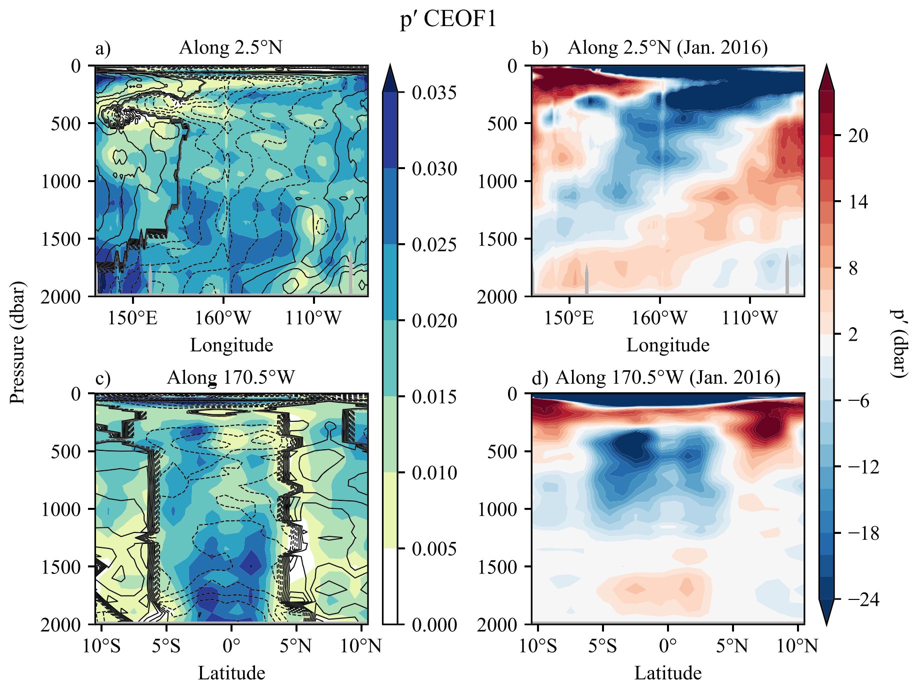

Figure 7. Isotherm displacement CEOF1 (a,c) amplitudes (colors) and spatial phases (contours; 30° intervals) and (b,d) the real parts of the CEOF1/PC1 reconstructions (dbar; colors) in January 2016 along (a,b) 2.5°N and (c,d) 170.5°W. The isotherm displacement CEOF1 vertical sections are constructed from the individual CEOF1s calculated on each pressure surface. CEOF = Complex Empirical Orthogonal Function; PC = Principal Component.

and both time-longitude and depth-time Hovmöller diagrams (Figures 8 and 9). CEOF1′s maximum amplitude (Figures 7a and 7c) occurs fairly deep (>1,000 dbar), suggesting a wave with a higher vertical mode than 1. Below 1,000 dbar, the amplitude maxima are also equatorially symmetric, while above 1,000 dbar, they occur on either side of the equator but are stronger in the south (Figure 7c). The reconstructed fields (Figure 7b and 7d) in January 2016 (when the Niño3.4 index is at a maximum) exhibit surface-intensified amplitudes that are strongest above 500 dbar. As expected for a vertically propagating Rossby wave, regions of positive and negative isotherm displacement anomalies track downward and westward (Figure 7b), and maximum correlations between the Niño3.4 index and the first PC across all pressure levels (not shown) generally decrease with depth while the lag increases, with values ranging from $|r|$ = ~0.9 and zero lag near the surface to $|r|$ = ~0.5 and a 21-month lag at 1,800 dbar. Hovmöller diagrams of the isotherm displacement CEOF1/PC1 reconstruction along 2.5°N at 1,000 dbar (Figure 8) and at 2.5°N and 170.5°W (Figure 9) reveal that the isotherm displacement anomalies propagate both westward (Figure 8) and upward (Figure 9) in time. Assuming a first meridional mode Rossby wave, using $N = 0.0022\ s^{-1}$ for the mean buoyancy frequency (Johnson, Sloyan, et al., 2002; Youngs & Johnson, 2015), and a period (24 months) estimated from the 200–2,000 dbar mean decorrelation timescale of PC1 yields a vertical mode of 3–4 for isotherm displacement CEOF1.

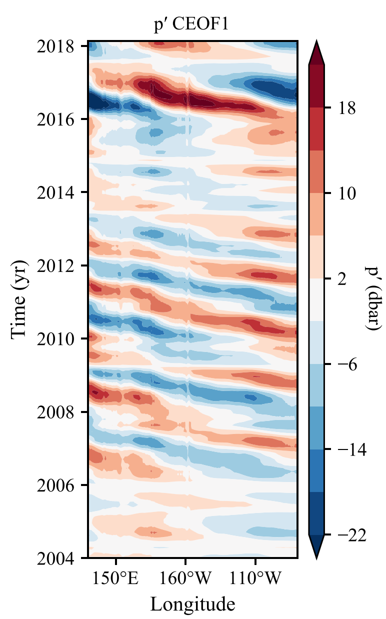

Figure 8. Hovmöller diagram of isotherm displacement CEOF1/PC1 reconstruction along 2.5°N at 1,000 dbar. Isotherm displacement CEOF1 has been multiplied by PC1 so that it has units of the original data (dbar). CEOF = Complex Empirical Orthogonal Function; PC = Principal Component.

Given the clear El Niño signals in isotherm displacement CEOF1 and PC1 across pressure levels, we might expect to find complementary patterns in one of the 1,000-dbar residual zonal velocity CEOFs and

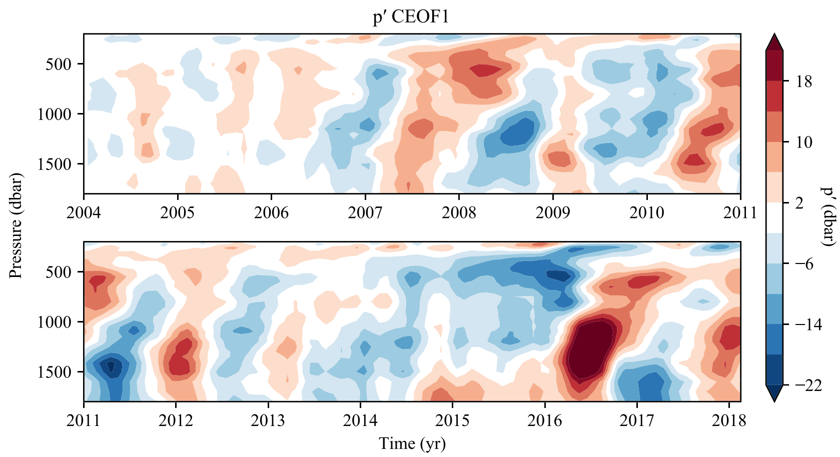

Figure 9. Hovmöller diagram of isotherm displacement CEOF1/PC1 reconstruction at 2.5°N, 170.5°W. Isotherm displacement CEOF1s across pressure levels have been multiplied by their corresponding PC1s so that the reconstruction has units of the original data (dbar). CEOF = Complex Empirical Orthogonal Function; PC = Principal Component.

PCs, but this is not the case (Figures S1 and S2). With strong amplitude along the equator and a coherent phase pattern that zonally spans the Pacific in about a year (Figure S1), zonal velocity CEOF1 is consistent with an interannual modulation of the annual Rossby wave, but any interpretation beyond this is uncertain. Both the first and second zonal velocity CEOFs exhibit a spatial structure and lower frequency variations that are not clearly related to the isotherm displacement CEOF1 and PC1 at 1,000 dbar, nor do they exhibit any robust patterns that can be cleanly connected to relevant physical processes such as ENSO.

4. Discussion and Conclusion

We use Argo float drift velocities at 1,000 dbar from Lebedev et al. (2007) and isotherm displacements derived from Roemmich and Gilson (2009), both updated through February 2018, to analyze physical state variables in the equatorial Pacific. The results we present for both the mean and seasonal cycle (Figures 1–4) are not novel but provide an update to previous results with additional data. Consistent with the findings of Cravatte et al. (2012, 2017) and others, the mean 1,000-dbar zonal velocity (Figure 1) comprises a series of alternating eastward and westward jets of small meridional scale (1–2°) that extend zonally across the basin. These are likely signatures of the Equatorial Intermediate Currents (e.g., Firing et al., 1998), near the equator, but clearly extend poleward with similar meridional scales. The zonal velocity and isotherm displacement seasonal cycles (Figures 2–4) indicate the presence of a vertically propagating annual Rossby wave, which has also been documented in previous observational and modeling studies (Johnson, Kunze, et al., 2002; Kessler & McCreary, 1993; Lukas & Firing, 1985; Yu & McPhaden, 1999; Yuan, 2005). The wave has a zonal velocity signature larger than the mean field around the equator in portions of the central and western equatorial Pacific, consistent with previous findings (e.g., Marin et al., 2010). With more observations available for our analysis, we are able to discern a coherent secondary maximum Rossby wave signature deep in the eastern portion of the basin predicted by a model (Kessler & McCreary, 1993), as well as report on more novel but weaker semiannual Rossby wave-like beams (Figure 4b; orange lines) in both the eastern and central portions of the basin.

In addition to analyzing the mean and seasonal cycle, we use CEOFs to examine the residual velocity and isotherm displacement variance. The main result from this analysis is that isotherm displacement CEOF1, calculated independently at each pressure level, is related to ENSO (Figures 5–7), with PC1 at each pressure level highly correlated with the Niño3.4 index. In accordance, isotherm displacement CEOF1 exhibits spatial patterns that are characteristic of an interannual modulation of the annual Rossby wave. At both 500 and 1,000 dbar, the signal is nearly basin-scale zonally with symmetric off-equator amplitude maxima (Figure 5). A depth-longitude snapshot of the CEOF1/PC1 reconstruction (Figure 7b) shows coherent patterns of positive and negative isotherm displacement anomalies that tilt downward and westward across the basin, while Hovmöller diagrams (Figures 8 and 9) show upward and westward phase propagation. CEOF1's amplitude maximum is fairly deep (>1,000 dbar; Figures 7a and 7c) and has a different pattern than the annual harmonic (Figure 4a), but the analysis still suggests a relatively low vertical mode. Calculations assuming first meridional mode Rossby wave physics, buoyancy frequency $N = 0.0022\ s^{-1}$, and a period of 24 months (the 200–2,000 dbar mean of the estimated PC1 decorrelation times) yield a vertical mode estimate of 3–4.

We expect that the forcing mechanism for the isotherm displacement interannual signals is analogous to that of the annual Rossby wave described in Kessler and McCreary (1993). However, instead of a signal that is forced by annual wind variations, the interannually varying signals we find here are likely forced by interannual wind variations associated with ENSO. Correlations between isotherm displacement PC1 at 1,000 dbar and NCEP/NCAR Reanalysis (Kalnay et al., 1996) monthly mean surface zonal winds (not shown) from January 2004 through February 2018 (averaged 5°S–5°N, 150°E–90°W) are fairly high (r = -0.5, 14-month lag), suggesting a connection between the surface wind (which in turn is highly correlated with the Niño3.4 index, r = 0.8 at a 2-month lag) and the deep isotherm displacement signals. The spatial and temporal patterns (Figures 5–9) we find are also similar to those in Kessler and McCreary (1993) except that our patterns are consistent with an interannual modulation of the annual Rossby wave rather than the annual Rossby wave itself.

While the interannual modulation of isotherm displacements, and their relation to ENSO, is fairly clear, this is not the case for the zonal velocity CEOFs (Figure S1). Other analyses or a longer time series may be required in order to better understand the residual zonal velocity variance. With strong amplitudes on the equator and spatially coherent phase that zonally spans the equatorial Pacific in about a year, velocity CEOF1 (Figure S1) is broadly consistent with an interannual modulation of the annual Rossby wave, but it is not obviously related to isotherm displacement CEOF1 on any pressure level or ENSO. It is thus not clear how to extract any meaningful information about the zonal velocity interannual variability or the physical processes that lead to the spatial patterns and low-frequency variability that we find. The robust isotherm displacement CEOF1 signals are somewhat at odds with this, as we would expect them to lead to equally strong and related zonal velocity variations. However, the zonal velocity record we employ here is fairly short (~10 years) and based on fewer data points than the isotherm displacements. Both of these factors may impact the CEOF results, especially for variability on interannual and longer timescales. Thus, it seems that at present, it is still necessary to await a longer observational time series or employ a model (e.g., Marin et al., 2010) to explore the residual zonal velocity variance.

Acknowledgments
The authors thank William Kessler for scientific discussions and two anonymous reviewers for comments that helped to improve the manuscript. The YoMaHa'07 data set is available at the APDRC website (http://apdrc.soest.hawaii.edu/projects/yomaha/). The Roemmich and Gilson Argo Climatology is available at the Scripps Institution of Oceanography website (http://sio-argo.ucsd.edu/RG_Climatology.html). NCEP Reanalysis Derived data is provided by the NOAA/OAR/ESRL PSD, Boulder, Colorado, USA, and is available at the ESRL website (https://www.esrl.noaa.gov/psd/). HZ is funded by the Joint Institute for the Study of the Atmosphere and Ocean (JISAO) under NOAA Cooperative Agreement NA15OAR4320063. GCJ was funded by the Climate Observation Division, Climate Program Office, National Oceanic and Atmospheric Administration (NOAA), the U.S. Department of Commerce and NOAA Research. All figures were created using Python's matplotlib plotting package (PMEL contribution number 4855).

References

Ascani, F., Firing, E., Dutrieux, P., McCreary, J. P., & Ishida, A. (2010). Deep equatorial ocean circulation induced by a forced–dissipated Yanai beam. *Journal of Physical Oceanography*. *40*(5), 1118–1142. https://doi.org/10.1175/2010JPO4356.1

Bouzinac, C., Vazquez, J., & Font, J. (1998). Complex empirical orthogonal functions analysis of ERS-1 and TOPEX/POSEIDON combined altimetric data in the region of the Algerian current. *Journal of Geophysical Research*, *103*(C4), 8059–8071. https://doi.org/10.1029/97JC02909

Chelton, D. B., Schlax, M. G., Lyman, J. M., & Johnson, G. C. (2003). Equatorially trapped Rossby waves in the presence of meridionally sheared baroclinic flow in the Pacific Ocean. *Progress in Oceanography*, *56*, 323–380. https://doi.org/10.1016/S0079-6611(03)00008-9

Cravatte, S., Kessler, W. S., & Marin, F. (2012). Intermediate zonal jets in the tropical Pacific Ocean observed by Argo floats. *Journal of Physical Oceanography*, *42*, 1475–1485. https://doi.org/10.1175/JPO-D-11-0206.1

Cravatte, S., Kestenare, E., Marin, F., Dutrieux, P., & Firing, E. (2017). Subthermocline and intermediate zonal currents in the tropical Pacific Ocean: Paths and vertical structure. *Journal of Physical Oceanographyr*, *47*, 2305–2324. https://doi.org/10.1175/JPO-D-17-0043.1

Davis, R. E. (1998). Preliminary results from directly measuring middepth circulation in the tropical and south Pacific. *Journal of Geophysical Research*, *103*(C11), 24,619–24,639. https://doi.org/10.1029/98JC01913

Davis, R. E. (2005). Intermediate-depth circulation of the Indian and south Pacific oceans measured by autonomous floats. *Journal of Physical Oceanography*, *35*(5), 683–707. https://doi.org/10.1175/JPO2702.1

Eriksen, C. C. (1981). Deep currents and their interpretation as equatorial waves in the western Pacific Ocean, *Journal of Physical Oceanography*, *11* (1), 48–70. https://doi.org/10.1175/1520-0485(1981)011¡0048:DCATIA¿2.0.CO;2

Eriksen, C. C. (1985). Moored observations of deep low-frequency motions in the central Pacific Ocean: Vertical structure and interpretation as equatorial waves. *Journal of Physical Oceanography*, *15* (8), 1085–1113. https://doi.org/10.1175/15200485(1985)015¡1085:MOODLF¿2.0.CO;2

Firing, E. (1987). Deep zonal currents in the central equatorial Pacific. *Journal of Marine Research*, *45*(4), 791–812. https://doi.org/10.1357/002224087788327163

Firing, E., Wijffels, S. E., & Hacker, P. (1998). Equatorial subthermocline currents across the Pacific. *Journal of Geophysical Research*, *103*(C10), 21,413–21,423. https://doi.org/10.1029/98JC01944

Gouriou, Y., Delcroix, T., & Eldin, G. (2006). Upper and intermediate circulation in the western equatorial Pacific Ocean in October 1999 and April 2000. *Geophysical Research Letters*, *33*, L10,603. https://doi.org/10.1029/2006GL025941

Hayes, S. P., & Milburn, H. B. (1980). On the vertical structure of velocity in the eastern equatorial Pacific, *Journal of Physical Oceanography*, *10* (4), 633–635. https://doi.org/10.1175/1520-0485(1980)010¡0633:OTVSOV¿2.0.CO;2

Johnson, G. C., Kunze, E., McTaggart, K. E., & Moore D. W., (2002). Temporal and spatial structure of the equatorial deep jets in the Pacific Ocean, *Journal of Physical Oceanography*, *32* (12), 3396–3407. https://doi.org/10.1175/1520-0485(2002)032¡3396:TASSOT¿2.0.CO;2

Johnson, G. C., Sloyan, B. M., Kessler, W. S., & Mctaggart, K. E. (2002). Direct measurements of upper ocean currents and water properties across the tropical Pacific during the 1990s, *Progress in Oceanography*, *52*(1), 31–61. https://doi.org/10.1016/S0079-6611(02)00021-6

Kalnay, E., M. Kanamitsu, R. Kistler, W. Collins, D. Deaven, L. Gandin, et al., 1996: The NCEP/NCAR 40-Year Reanalysis Project. *Bulletin of the American Meteorological Society*, *77*, 437–472, https://doi.org/10.1175/1520-0477(1996)077<0437:TNYRP>2.0.CO;2

Kessler, W. S., & McCreary, J. P. (1993). The annual wind-driven Rossby wave in the subthermocline equatorial Pacific, *Journal of Physical Oceanography*, *23* (6), 1192–1207. https://doi.org/10.1175/1520-0485(1993)023¡1192:TAWDRW¿2.0.CO;2

Lebedev, K. V., Yoshinari, H., Maximenko, N. A., & Hacker, P. W. (2007). YoMaHa'07: Velocity data assessed from trajectories of Argo floats at parking level and at the sea surface, IPRC Tech. *Rep*, *4*(2).

Leetmaa, A., & Spain, P. F. (1981). Results from a velocity transect along the equator from 125 to 159°W, *Journal of Physical Oceanography*, *11* (7), 1030–1033. https://doi.org/10.1175/15200485(1981)011¡1030:RFAVTA¿2.0.CO;2

Lukas, R., & Firing, E. (1985). The annual Rossby wave in the central equatorial Pacific Ocean, *Journal of Physical Oceanography*, *15* (1), 55–67. https://doi.org/10.1175/15200485(1985)015¡0055:TARWIT¿2.0.CO;2

Marin, F., Kestenare, E., Delcroix, T., Durand, F., Cravatte, S., Eldin, G., & Bourdallé-Badie, R. (2010). Annual reversal of the equatorial intermediate current in the Pacific: Observations and model diagnostics. *Journal of Physical Oceanography*, *40*, 915–933. https://doi.org/10.1175/2009JPO4318.1

Qiu, B., Rudnick, D. L., Chen, S., & Kashino, Y. (2013). Quasi-stationary north equatorial undercurrent jets across the tropical north Pacific Ocean. *Geophysical Research Letters*, *40*, 2183–2187. https://doi.org/10.1002/grl.50394

Ridgway, K.R., Dunn, J.R., & Wilkin, J. L. (2002). Ocean interpolation by four-dimensional weighted least squares—Application to the waters around Australasia. *ournal of Atmospheric and Oceanic Technology*, *19*, 1357–1375. https://doi.org/10.1175/1520-0426(2002)019<1357:OIBFDW>2.0.CO;2

Roemmich, D., & Gilson, J. (2009). The 2004–2008 mean and annual cycle of temperature, salinity, and steric height in the Global Ocean from the Argo program. *Progress in Oceanography*, *82*(2), 81–100. https://doi.org/10.1016/j.pocean.2009.03.004

Rowe, G. D., Firing, E., & G. C. Johnson (2000). Pacific equatorial sub-surface countercurrent velocity. transport, and potential vorticity, *Journal of Physical Oceanography*, *30* (6), 1172–1187. https://doi.org/10.1175/1520-0485(2000)030¡1172:PESCVT¿2.0.CO;2

Stramma, L., Johnson, G. C., Firing, E., & Schmidtko, S. (2010). Eastern Pacific oxygen minimum zones: Supply paths and multidecadal changes. *Journal of Geophysical Research*, *115*. https://doi.org/10.1029/2009JC005976

Taft, B., Hickey, B., Wunsch, C., & Baker, D. (1974). Equatorial undercurrent and deeper flows in the central Pacific. *Deep Sea Research and Oceanographic Abstracts*, *21*(6), 403–430. https://doi.org/10.1016/0011-7471(74)90091-6

Voorhis, A., Luyten, J. R., Needell, G., & Thomson, J. (1984). Wind-forced variability of upper ocean dynamics in the central equatorial Pacific during PEQUOD, *Journal of Physical Oceanography*, *14* (3), 615–622. https://doi.org/10.1175/1520-0485(1984)014¡0615:WFVOUO¿2.0.CO;2

Wyrtki, K., & Kilonsky, B. (1984). Mean water and current structure during the Hawaii-to-Tahiti Shuttle experiment, *Journal of Physical Oceanographyx*, *14* (2), 242–254, https://doi.org/10.1175/1520-0485(1984)014¡0242:MWACSD¿2.0.CO;2

Youngs, M. K., & Johnson, G. C. (2015). Basin-wavelength equatorial deep jet signals across three oceans. *Journal of Physical Oceanography*, *45*(8), 2134–2148. https://doi.org/10.1175/JPO-D-14-0181.1

Yu, X., & McPhaden, M. J. (1999). Seasonal variability in the equatorial Pacific, *J. Phys. Oceanogr*, *29* (5), 925–947. https://doi.org/10.1175/1520-0485(1999)029¡0925:SVITEP¿2.0.CO;2

Yuan, D. (2005). Role of the Kelvin and Rossby waves in the seasonal cycle of the equatorial Pacific Ocean circulation. *Journal of Geophysical Research*, *110*. https://doi.org/10.1029/2004JC002344